JOURNAL OF MATERIALS SCIENCE 32 (1997) 47–56

Fabrication of particulate reinforced magnesium composites by applying a spontaneous infiltration phenomenon

HIROMITSU KANEDA
Group III, Development Department II, Suzuki Motor Corporation, Hamamatsu-nishi P.O. Box 1, Hamamatsu, 432-91, Japan

TAKAO CHOH
Department of Materials Processing Engineering, School of Engineering, Nagoya University, Furo-cho, Chikusa-ku, Nagoya, 464-01, Japan

A new fabrication method of particulate reinforced magnesium matrix composites using a spontaneous infiltration phenomenon was developed. By mixing infiltration agent powder with reinforcement powder, the magnesium melt spontaneously infiltrated into the powder mixture. In this study, pure magnesium, SiO_2 and SiC particle (SiC_p, 1.2, 2, 3, 4 and 8 μm) powders were used as the matrix metal, infiltration agent and reinforcements, respectively. Experiments to clarify the conditions in which the spontaneous infiltration occurred were carried out under pure argon atmosphere at 973 K. Furthermore, the infiltration velocity was measured. Spontaneous infiltration occurred in the 2, 3, 4 and 8 μm SiC_p systems. A minimum SiO_2 content necessary for spontaneous infiltration existed and it depended on SiC_p diameter. Microstructural observation of the composites revealed that SiC_p dispersed homogeneously, even though the diameter of SiC_p was fine, and MgO and Mg_2Si reaction products were observed. During infiltration, a temperature rise was observed, caused by Mg–SiO_2 thermit reaction. Consequently, spontaneous infiltration was caused by improvement of wettability between the magnesium melt and SiC_p, which resulted from Mg–SiO_2 thermit reaction at the infiltration front.

1. Introduction

Magnesium and magnesium alloy matrix composites have various advantages [1], such as low specific weight, high specific strength, high elastic modulus and high wear resistance [2], because these matrices are the lightest metals in practical structural alloys. Environmental problems have become serious in the world, so the application of light metals and their composites for structural materials has been noticed by the automobile industry [3].

There are many methods for fabrication of particulate reinforced metal matrix composites (MMCs), such as the vortex method, compo-casting [4], powder metallurgy (PM), and so on. In the case of aluminum MMCs, the vortex method is commercially used by ALCAN [5], and is a good proof of cost effectiveness. However, for fabrication of magnesium matrix composites, it is generally said that squeeze casting and the PM method, rather than the vortex method, are suitable [6]. One of the greatest reasons is that magnesium, particularly its melt, is so active that many defects, such as an oxide or other reaction products, are introduced into the composite during the fabrication process [4], and these degrade the properties of the product.

In the field of aluminum matrix composites, a pressureless infiltration process [7–10] has been developed. This process is an effective method for obtaining sound composite materials. However, there have been few studies applying a spontaneous infiltration phenomenon to the fabrication of magnesium matrix composites.

The authors attempted to apply this phenomenon to the fabrication of SiC particulate reinforced magnesium matrix composites. Consequently, by mixing SiO_2 powder with reinforcement powder, the magnesium melt spontaneously infiltrated into the powder mixture. This process has many advantages for the fabrication of magnesium MMCs, such as relatively low process temperature, short incorporation time and no defects. In this study, experiments to find out the conditions in which spontaneous infiltration occurred were carried out under pure argon atmosphere at 973 K. In addition, the infiltration-front temperature and the infiltration velocity were measured.

2. Experimental procedure

2.1. Materials

Pure magnesium (99.97%) is used for the matrix metal, in order to simplify discussions about microstructural analysis, reaction products and the infiltration mechanism. The feature of this study is previous mixing of the SiO_2 powder (average diameter: $\bar{d} = 2$ μm,

0022–2461

α-quartz) infiltration agent with the reinforcement powder. Powders are mixed in a mortar with very little ethanol to avoid agglomeration. Five kinds of SiC_p powders with different average diameters are used as reinforcements, which are commercially used for polishing abrasive.

Table I shows the average diameters of the SiC_p powders and the contents of the SiO_2 powder (mass %) in powder mixtures for the experiments to find out the conditions necessary for spontaneous infiltration.

TABLE I SiO_2 contents mixed with SiC_p powders with various diameters

SiC_p diameter (μm)	SiO_2 content (mass %)						
1.2	0			7	15	23	31
2.0	0			7	15	23	31
3.0	0		3.5	7	15	23	31
4.0	0	2.1	3.5	7	15	23	31
8.0	0	2.1	3.5	7	15	23	31

2.2. Apparatus

All the experiments are carried out using an induction furnace in a chamber. Fig. 1 shows the experimental setup for the spontaneous infiltration experiment. A steel crucible as a heat source is set in the centre of an induction coil, and then two alumina crucibles (99.5% Al_2O_3 and 0.1% SiO_2) are set in it. One crucible containing a thermocouple and pure magnesium is used as a dummy to control the temperature of the furnace. Another crucible with two small holes at the bottom contains a sample with 4 g pure magnesium and 1.6 g of the powder mixture. In addition, to examine the effects of these bottom holes, crucibles without holes were also employed.

2.3. Spontaneous infiltration experiments

Experiments were carried out to find out the conditions necessary for spontaneous infiltration.

The chamber with a sample and a dummy crucible was evacuated, and these were heated up to approximately 600 K. Then, the chamber was purged with pure argon gas until atmospheric pressure, the temperature was raised to 973 K and held for 20 min. After that, the sample was cooled in a chamber until 500 K, and was taken out. The specimen was visually examined to see whether spontaneous infiltration had occurred.

2.4. Measurement of infiltration-front temperature and infiltration velocity

The infiltration-front temperature was measured in the systems underlined on Table I, by setting three thermocouples fixed by alumina cement through holes on the side of the crucible. The arrangement of the three thermocouples is illustrated in Fig. 2. These are called TC1, TC2 and TC3 from top to bottom. The changes in temperature of the thermocouples during infiltration were recorded. The data are also utilized for evaluation of infiltration velocity. The velocity between TC1 and TC3 is defined by measuring the time interval of each thermocouple temperature change.

2.5. Analysis

To analyse the spontaneous infiltration mechanism, optical microscope observation, X-ray diffraction (XRD) analysis and electron probe microanalysis (EPMA) were carried out.

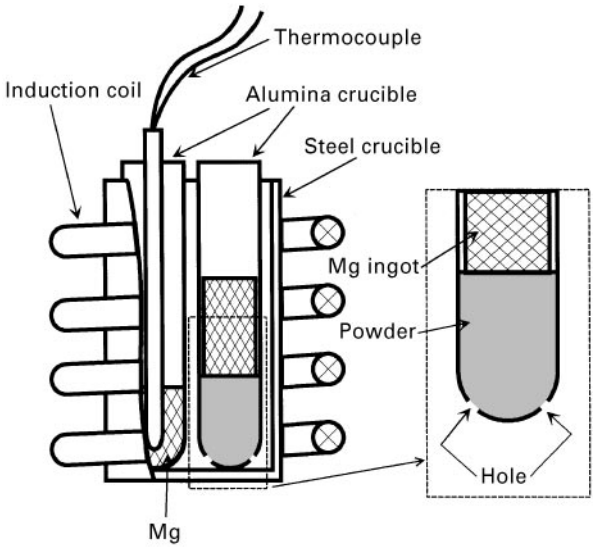

Figure 1 Experimental setup for spontaneous infiltration.

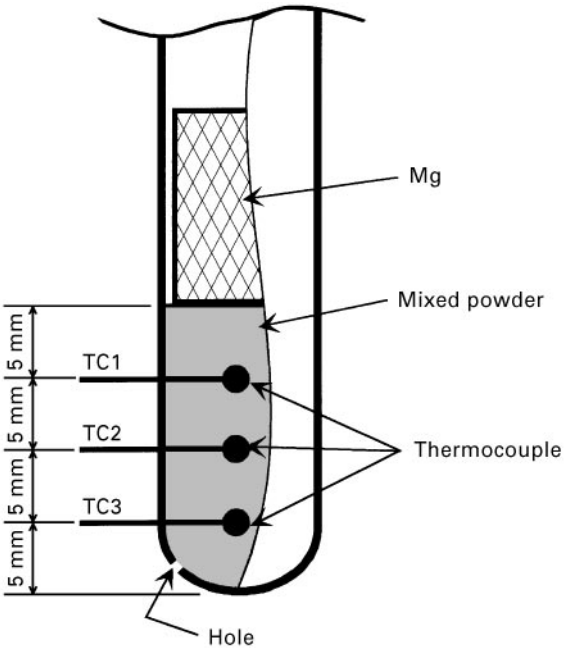

Figure 2 Schematic illustration of thermocouple setup in crucible.

3. Results

3.1. Macroscopic observation

Fig. 3 shows the appearance and a vertical section of the spontaneously infiltrated sample. The powder system was SiC_p(3 μm) + 23 mass % SiO_2, and a crucible

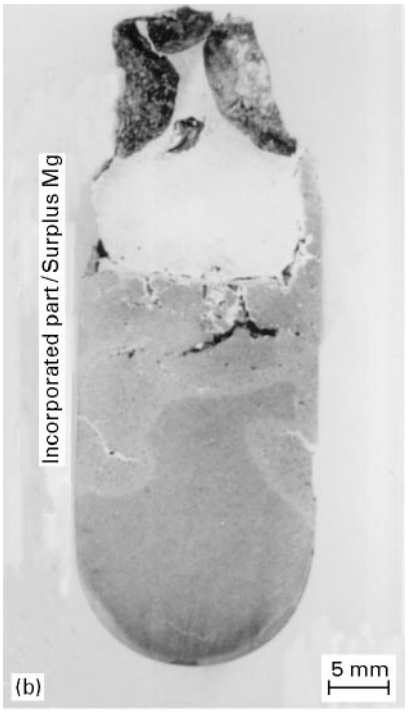

Figure 3 Appearance (a) and vertical section (b) of spontaneously infiltrated magnesium composite using an SiC_p (3 μm) + 23 mass % SiO_2 powder system.

with two holes at the bottom was used. The figure indicates that magnesium melt infiltrated spontaneously and incorporation was completed.

In Fig. 3b, the light part of the section shows the surplus magnesium, and the grey is the incorporated part, which has two areas: light grey and dark grey. These are later described in the section on microstructural observation. The infiltrated area does not have any un-infiltrated parts in all of the cases that were completely infiltrated up to the bottom of the crucible. But open parts were sometimes seen in the infiltrated samples. It is supposed that the defects correspond to

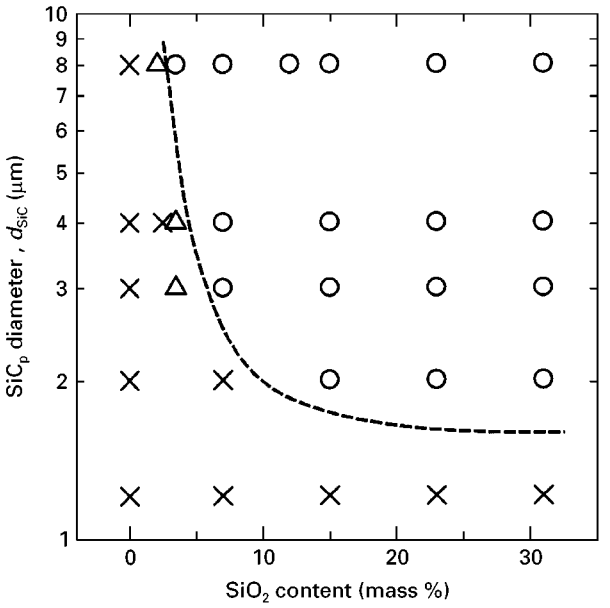

Figure 4 Effects of SiO_2 content and reinforcement particle diameter on spontaneous infiltration.

the part not filled by powder formed by large powder agglomerates when powder materials filled the crucible.

3.2. SiO_2 content necessary for spontaneous infiltration

The SiO_2 contents in the powder mixtures necessary for completion of spontaneous infiltration were measured for various SiC_p diameters. The results are shown in Fig. 4: (○) denotes complete infiltration to the bottom of the crucible, (△) denotes incomplete infiltration and (×) denotes no infiltration. A broken line is drawn on the boundary between complete and incomplete infiltration systems.

This result puts forth two important facts. One is that no infiltration is observed in the system without SiO_2, i.e. the infiltration agent is a requisite for spontaneous infiltration. Another is that the SiO_2 content necessary for completion of spontaneous infiltration (called the minimum SiO_2 content) changes according to the SiC_p diameter. Namely, the minimum SiO_2 content increases with decreasing SiC_p diameter. For instance, 15 mass % SiO_2 is necessary in 2 μm SiC_p system, while the 8 μm SiC_p system needs only 3.5 mass % SiO_2. No infiltration was observed in the 1.2 μm SiC_p system.

The necessity of holes on the bottom of the crucible was confirmed for a few systems (mainly the 3 μm SiC_p system) in which complete infiltration has already been observed. Consequently, no infiltration occurred in the crucible without a hole in its bottom.

3.3. Microstructural observation

Fig. 5 shows photomicrographs of composites obtained by the spontaneous infiltration process; (a) and (b) are for the Mg + 3 μm SiC_p + 7 mass % SiO_2 system, and (c) and (d) are for the Mg + 3 μm SiC_p

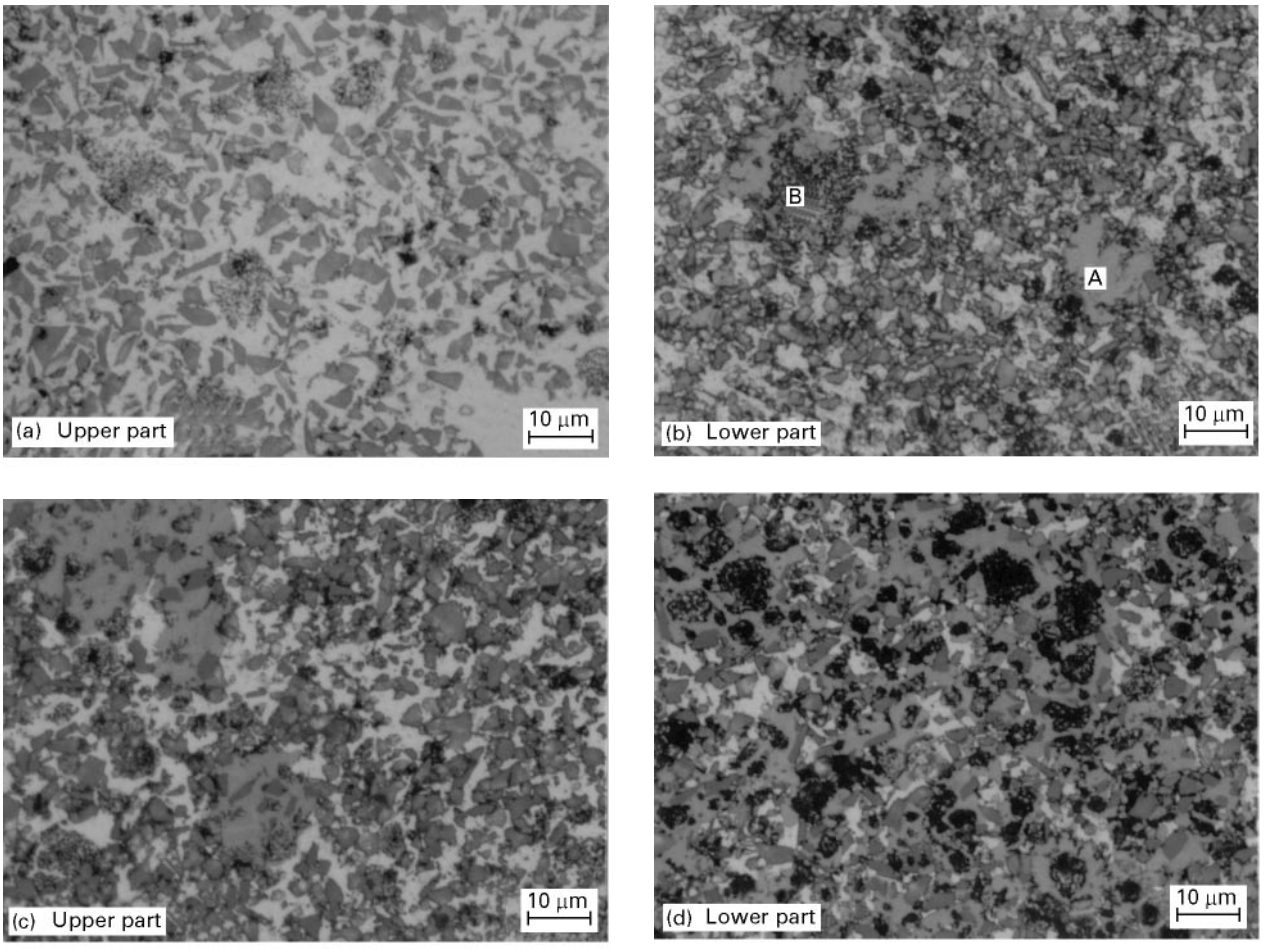

Figure 5 Microstructures of composites fabricated by the spontaneous infiltration process: (a) and (b) Mg + 3 μm SiC_p + 7 mass % SiO_2, and (c) and (d) Mg + 3 μm SiC_p + 31 mass % SiO_2. (a) and (c) show upper parts, and (b) and (d) show lower parts.

+ 31 mass % SiO_2 system. Homogeneous SiC_p distribution and a few pores were observed even though the SiC particles were fine and no agitation was applied.

These photographs signify that two products (marked A and B in Fig. 5b) exist in the composites. These are obviously reaction products between SiO_2 and the magnesium melt, because the quantities of these products in the 31 mass % SiO_2 system are much more than that in the 7 mass % system. The morphologies of these two products are different; phase A is relatively large and phase B looks like agglomerates of very fine particles. The distribution behaviours of phases A and B are also different. Phase A is mainly observed in the lower part, showing macrosegregation (Fig. 5a and b). This segregation corresponds to the dark grey area in Fig. 3b. In contrast, phase B does not have such a segregation tendency.

3.4. XRD and EPMA analyses

In order to identify the primary reaction products, XRD and EPMA analyses were carried out. Fig. 6 shows the scanning electron image and EPMA elemental maps of reaction products in the Mg + 3 μm SiC_p + 15 mass % SiO_2 system. Magnesium and silicon images were detected in phase A, while magnesium and oxygen images were detected in phase B.

Furthermore, from the X-ray diffraction patterns of the infiltrated internal part and the mixed powder shown in Fig. 7, it is found that Mg_2Si and MgO are detected in the composites, while the SiO_2 peak, which is indicated in the pattern of the mixed powder, is not detected. From these results, it is concluded that the reaction products, phases A and B, are Mg_2Si and MgO, respectively.

The reactions to form MgO and Mg_2Si from Mg and SiO_2 are as follow

$$2Mg + SiO_2 \rightarrow \underline{Si} + 2MgO \quad (1)$$

$$2Mg + \underline{Si} \rightarrow Mg_2Si \quad (2)$$

When the Si content in the magnesium melt is less than its solubility, reaction following Equation 1 occurs at the infiltration front. Then, when the Si content exceeds the solubility, the reaction in Equation 2 occurs simultaneously.

Considering the crystallization behaviour of Mg_2Si, the process of macrosegregation formation is explained. As Si dissolves into the magnesium melt at the infiltration front, the Si content near there becomes higher than in the inner part. Furthermore, the Si content at the infiltration front increases as the infiltration front proceeds. By this heterogeneous Si content, therefore, macrosegregation is formed.

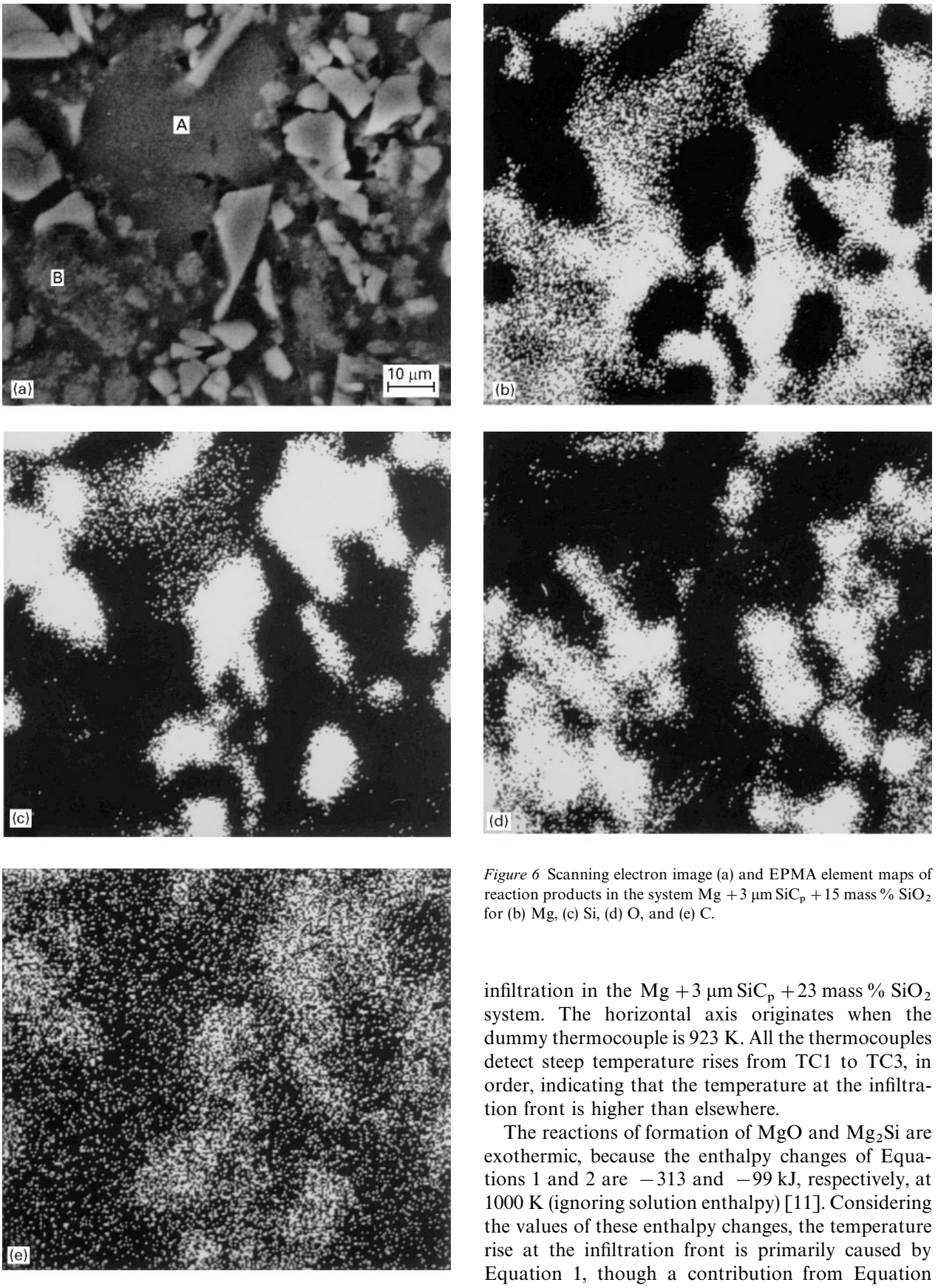

Figure 6 Scanning electron image (a) and EPMA element maps of reaction products in the system Mg $+3$ μm SiC_p $+15$ mass % SiO_2 for (b) Mg, (c) Si, (d) O, and (e) C.

3.5. Measurement of infiltration-front temperature

The infiltration-front temperature was measured by thermocouples to confirm the rise in temperature. Fig. 8 shows a typical time–temperature chart during infiltration in the Mg $+3$ μm SiC_p $+23$ mass % SiO_2 system. The horizontal axis originates when the dummy thermocouple is 923 K. All the thermocouples detect steep temperature rises from TC1 to TC3, in order, indicating that the temperature at the infiltration front is higher than elsewhere.

The reactions of formation of MgO and Mg_2Si are exothermic, because the enthalpy changes of Equations 1 and 2 are -313 and -99 kJ, respectively, at 1000 K (ignoring solution enthalpy) [11]. Considering the values of these enthalpy changes, the temperature rise at the infiltration front is primarily caused by Equation 1, though a contribution from Equation 2 probably exists.

The peak temperature may be near to the infiltration-front temperature, although the measured temperature is somewhat lower than the actual temperature, because the infiltration front moves with some velocity and the thermocouple tip has some thermal capacity. Fig. 9 shows the effects of both SiO_2 content and SiC_p diameters on the measured

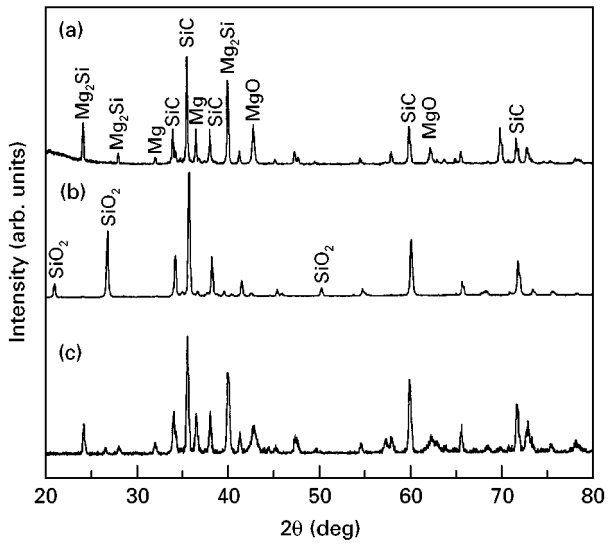

Figure 7 X-ray diffraction patterns of (a) the internal part of the composite, (b) the mixed powder and (c) the infiltration front in the 3 μm SiC_p + 23 mass % SiO_2 powder system.

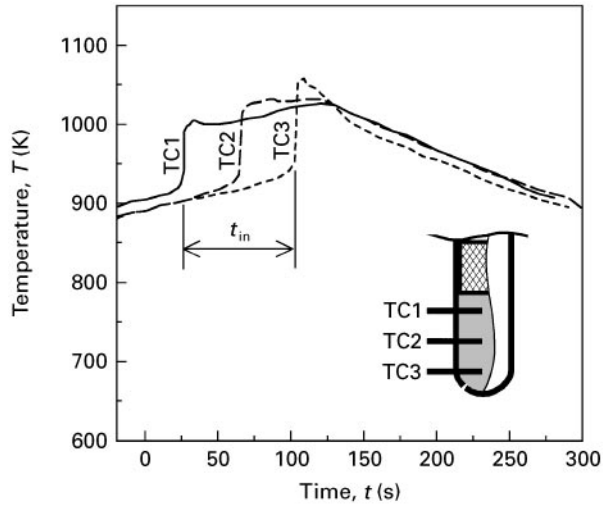

Figure 8 An example of the time–temperature chart during infiltration in the system Mg + 3 μm SiC_p + 23 mass % SiO_2.

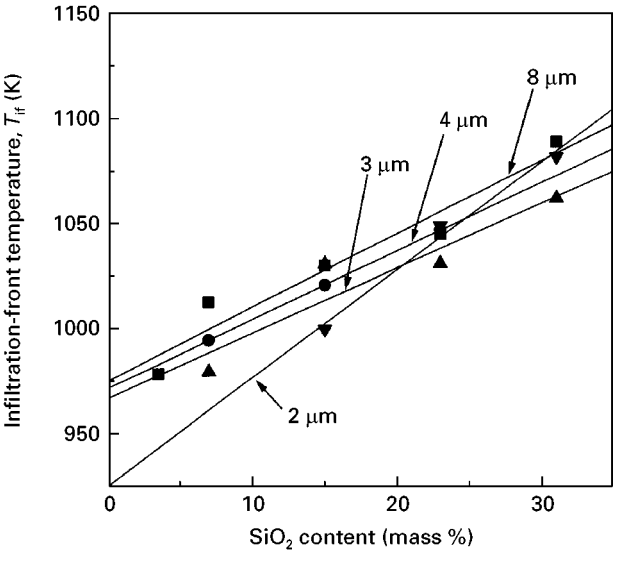

Figure 9 Effects of SiO_2 content and SiC particle diameters on the infiltration-front temperatures and least-square fit lines. SiC_p diameters: (■) 8 μm, (●) 4 μm, (▲) 3 μm, (▼) 2 μm.

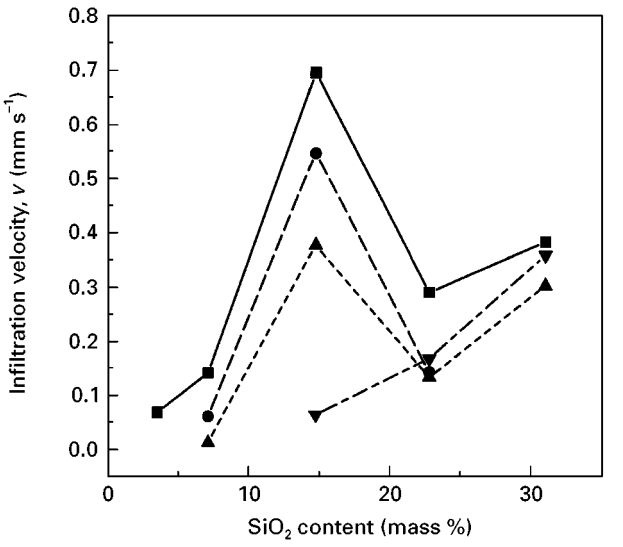

Figure 10 Effects of SiO_2 content and SiC_p diameter at (■) 8 μm, (●) 4 μm, (▲) 3 μm, (▼) 2 μm on the infiltration velocity.

infiltration-front temperatures. Each temperature is the average value of three thermocouples. Least-square fitted lines are also drawn for each SiC particle diameter (8, 4, 3 and 2 μm). The coefficients of correlation are 0.97, 1.00, 0.93 and 0.99, respectively, and show good fit. This figure indicates that the infiltration-front temperature is influenced by both SiO_2 content and SiC_p diameter and increases linearly with increasing SiO_2 content, although the gradient of the 2 μm SiC_p line is different. Moreover, this temperature decreases with decreasing SiC_p diameter, probably owing to differences in infiltration velocities and SiC_p specific areas.

3.6. Infiltration velocity

In this study, the average infiltration velocity between TC1 and TC3 was obtained by taking the interval time, t_{in}, shown in Fig. 8. The infiltration velocity is plotted against SiO_2 content in Fig. 10. The infiltration velocity has a maximum value at 15 mass % SiO_2, e.g. 0.7 mm s^{-1} is obtained for 8 μm SiC_p. It is also obvious from Fig. 10 that the velocity is influenced by both the SiO_2 content and the SiC_p diameter. Concerning the SiC_p diameter, the infiltration velocity increases with increasing SiC_p diameter below 15 mass % SiO_2 above this content, its effect on velocity becomes smaller. On the other hand, the effect of SiO_2 content is complex, as the velocity increases with SiO_2 content until 15 mass % SiO_2, and then steeply decreases. Because this tendency conflicts with the results of the infiltration-front temperature above this content, other velocity control factors should be considered.

4. Discussion

4.1. Spontaneous infiltration mechanism

The spontaneous infiltration mechanism of this study is discussed. The equation for spontaneous infiltration is generally well known, and it is also obtained by

putting some conditions into the equation about the pressure infiltration given by the Young–Kelvin law or Martins and coworkers [12, 13], as follows

$$\frac{2\gamma_{lv}\cos\theta}{r} + \rho g h_0 > 0 \quad (3)$$

where γ_{lv} is the liquid–vapour interfacial tension, θ is the contact angle, r is the hydraulic radius, ρ is the density of the liquid, g is the acceleration due to gravity, and h_0 is the initial height of the liquid. This equation indicates that θ should be equal to or less than 90° because of the low density of magnesium.

Considering the experimental results of complete infiltration, the apparent contact angle between the magnesium melt and the mixed powder, under the present experimental conditions, is less than or equal to 90°. Probably, this results from good wettability between the magnesium melt and SiO_2 and/or subsequent magnesium melt–SiO_2 exothermic reaction. In any case, the important thing is contact of the magnesium melt with SiO_2 to react. In this paper, the Mg–SiO_2 reaction is discussed principally, because this reaction occurs furiously and finishes in a moment with a bright white flash of light when the SiO_2 powder contacts with the magnesium melt directly.

The Mg–SiO_2 reaction of Equation 1 is called a thermit reaction, and has various effects on the system.

1. Silicon from reduced SiO_2 dissolves into the magnesium melt and the melt becomes an Mg–Si alloy.

2. Mg–SiO_2 thermit reaction heats the infiltration front.

The former probably decreases the wettability between the melt and SiC, because of alloying silicon. Although no contact angle data are obtained in the Mg–Si melt–SiC system, the wettability can be referred from Lim and Choh [14]. They measured the incorporation time of SiC_p powder into the Mg–Si alloy melt up to 10 mass % Si by a melt stirring method, and described that the incorporation time increased with Si content up to 4 mass % and then became constant. This result proves that Si alloying does not improve wettability between the magnesium melt and SiC.

The latter effect, therefore, is more important, because wettability is improved at a higher temperature in general.

To confirm these effects, two experiments were carried out. One used a pure magnesium matrix and a powder without SiO_2 at 1273 K. The other used an Mg–1.5 mass % Si alloy matrix and a powder without SiO_2 at 973 K. The other experimental conditions were the same. Consequently, spontaneous infiltration was observed only in the former case, though many defects were included. Hence, it is considered that spontaneous infiltration is caused by high temperature at the infiltration front resulting from Mg–SiO_2 thermit reaction.

The relationship between the minimum SiO_2 content and the SiC_p diameter is discussed. According to the results, increasing SiC_p diameter decreases the minimum SiO_2 content. Noting the infiltration-front temperature in the system 15 mass % SiO_2 (see Fig. 9), the temperature of the 2 μm SiC_p is lower than the others. This is caused by a decrease of the reaction quantity in unit time, i.e. the infiltration velocity. In addition, it should be taken into account that the specific area increases with decreasing SiC_p diameter. So the minimum SiO_2 content means the content that is necessary for maintaining the infiltration front at a high enough temperature during infiltration.

4.2. Effects of relative particle sizes of SiC and SiO_2

Considering the 1.2 μm SiC_p case, spontaneous infiltration was not observed, even with twice the content of SiO_2 powder compared with that of the 2 μm SiC_p case. In this section, contact of the magnesium melt with SiO_2 is discussed.

Fig. 11 shows the particle diameter distributions of SiO_2 and SiC_p powders used in this study. This figure indicates that all of the SiO_2 particles are larger than the 1.2 μm SiC particles. Generally, in the powder including two or more kinds of particle diameters, the smaller particles surround the larger particles because of absorption. SiO_2 particles are, therefore, surrounded by SiC particles in the case of the 1.2 μm SiC. Fig. 12 illustrates schematically the effect of relative particle size. In the case of Fig. 12a, i.e. for $d_{SiC_P} > d_{SiO_2}$, the magnesium melt establishes contact with reactive SiO_2 and infiltration initiates. In contrast, in the case of Fig. 12b, i.e. for $d_{SiC_P} < d_{SiO_2}$, infiltration does not initiate, because inactive SiC particles surround the SiO_2 particles, disturbing contact of the magnesium melt with SiO_2. It is supposed that this is the reason why spontaneous infiltration did not occur in the 1.2 μm SiC_p case.

Furthermore, the different tendencies of the infiltration velocity and the infiltration-front temperature in the 2 μm SiC_p system (in particular, 15 mass % SiO_2) can be explained. This system has a mixed mode with

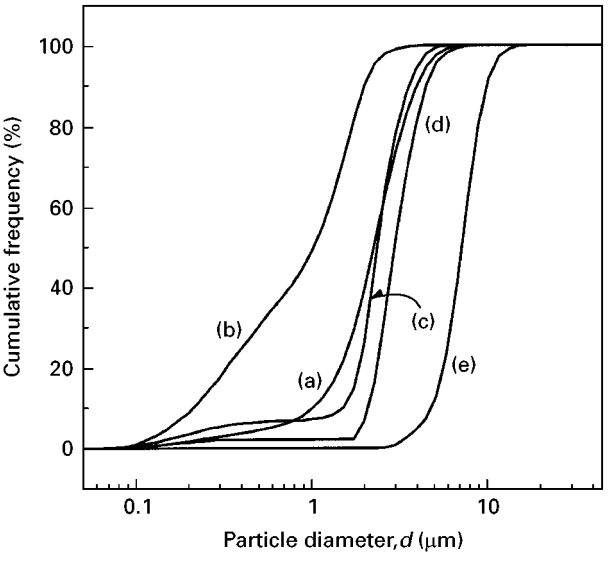

Figure 11 Particle diameter distributions of SiO_2 (a) and SiC_p powders (b–e) used. SiC_p diameters: (b) 1.2 μm, (c) 2 μm, (d) 3 μm, (e) 8 μm.

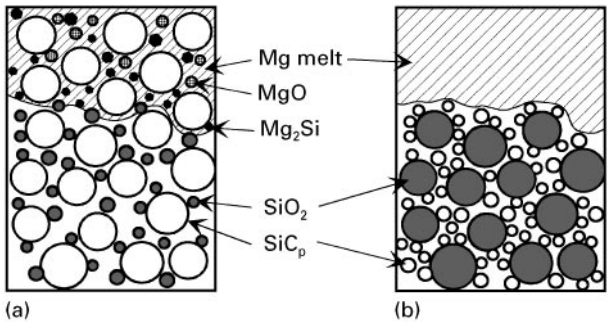

Figure 12 Effect of relative sizes of SiC and SiO_2 particles on (a) spontaneous infiltration, $d_{SiC_P} > d_{SiO_2}$, and (b) no infiltration, $d_{SiC_P} < d_{SiO_2}$.

Fig. 12a and b, considering the particle diameter distributions of 2 μm SiC_p and SiO_2 shown in Fig. 11. Only the SiO_2 particles smaller than SiC particles can react effectively at the infiltration front.

4.3. Infiltration velocity

As shown in Fig. 10, the infiltration velocity has a complex tendency with SiO_2 content. Considering only the infiltration-front temperature, at least the infiltration velocity should not decrease. However, it increased with increasing SiO_2 content up to 15 mass %, and then decreased steeply.

Now, to discuss this behaviour, the factors controlling the infiltration velocity are considered. The relation between infiltration height in the capillary, h, and time, t, is obtained from the Hagen–Poiseuille law, and is introduced by Semlak and Rhines [15] for a flow of molten metal into a powder mass. The equation is expressed as

$$h^2 = Ct$$

(where C is a constant) so the infiltration velocity, ν, is given as

$$\nu = \frac{C}{2h} \tag{4}$$

In the case of the rise of a liquid through a powder mass [15], C is described as

$$C = \frac{2}{\pi}\left(\frac{r\gamma_{lv}\cos\theta}{2\eta}\right) \tag{5}$$

where η is the viscosity.

It is difficult to discuss this from the view-point of viscosity, because there are little data on Mg–Si alloy viscosities. Furthermore, the Si content in the matrix metal always changes with the proceeding infiltration front. Hence, the infiltration velocity is discussed from the standpoint of the effect of SiC_p diameter, because the hydraulic radius, r, is defined by the SiC_p diameter at a certain SiO_2 content. Therefore, the effects of SiC_p diameter and reaction products on the infiltration velocity are discussed in the following section.

4.3.1. Effect of SiC_p diameter, i.e. hydraulic radius

Table II shows the hydraulic radii calculated from measurement results of apparent volumes of powder mixtures, using the expression

$$r = \frac{d\phi}{6\lambda(1-\phi)} \tag{6}$$

where d is the average particle diameter, φ is the porosity, and λ is the geometry factor that depends on the geometry of both particulate and capillary channels. A value of 1.42 is used as λ [16], and the existence of SiO_2 in mixed powder is neglected because it is consumed by magnesium. This table indicates that hydraulic radii for certain SiO_2 contents increase with increasing SiC_p diameters: e.g. in 15 mass % SiO_2, the hydraulic radii are 1.0, 1.5, 1.8 and 3.1 μm for 2, 3, 4 and 8 μm SiC_p, respectively, resulting in differences in infiltration velocities with SiC_p diameters. However, the steep drop in the infiltration velocity above 15 mass % SiO_2 cannot be explained from the effect of the hydraulic radius.

TABLE II Measured SiC_p volume fractions and calculated hydraulic radii of powder mixtures with various SiC_p diameters and SiO_2 contents

SiC_p diameter (μm)	SiO_2 content (mass %)	Measured SiC_p volume fraction (vol %)	Calculated hydraulic radius (μm)
2	15.0	18	1.0
2	23.0	16	1.2
2	31.0	16	1.3
3	7.0	20	1.4
3	15.0	19	1.5
3	23.0	17	1.7
3	31.0	16	1.9
4	7.0	22	1.7
4	15.0	20	1.8
4	23.0	19	2.1
8	3.5	27	2.6
8	7.0	25	2.8
8	15.0	23	3.1
8	23.0	21	3.6
8	31.0	19	4.0

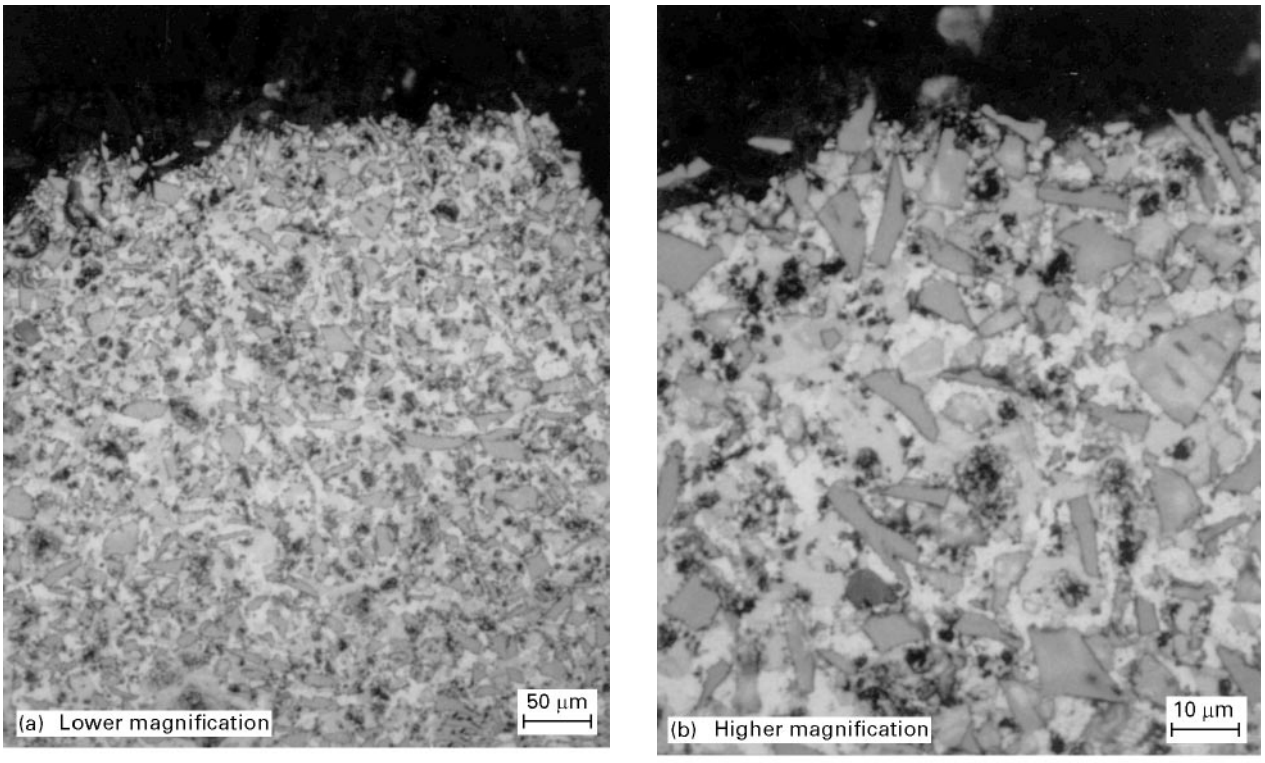

Figure 13(a, b) Photomicrographs of an infiltration front that is interrupted by water-quenching during infiltration in the system Mg + 8 μm SiC_p + 23 mass % SiO_2.

4.3.2. Effects of Mg–SiO_2 reaction products, MgO and Mg_2Si

MgO was homogeneously dispersed on a macroscopic scale. Considering its crystallization behaviour, MgO must crystallize just after reaction at the infiltration front and must stay near the position of crystallization, because its melting point is much higher than the infiltration-front temperature. This behaviour is proved by microstructural observation, because macrosegregation was not observed. Therefore, it is considered that the formation of MgO is one disturbing factor, and it decreases the infiltration velocity for different SiC_p diameters above 15 mass % SiO_2. However, the steep drop in the infiltration velocity above 23 mass % SiO_2 cannot be explained by the disturbing effect of MgO, because the quantity of MgO, or the degree of such disturbance, must increase linearly with increasing SiO_2 content.

The influence of Mg_2Si crystallization is considered. The important thing is whether Mg_2Si crystallizes at the infiltration front during the process. To confirm this, the microstructure of the infiltration front was observed, shown in Fig. 13, for a specimen water-quenched during infiltration. The system is Mg + 3 μm SiC_p + 23 mass % SiO_2; the content corresponds to the steep drop in the infiltration velocity. In this figure, white, light grey, dark grey, and black parts correspond to matrix metal, Mg_2Si, SiC and MgO, respectively. Hence, Fig. 13 indicates that Mg_2Si crystallizes near the infiltration front above the SiO_2 content. Furthermore, unreacted SiO_2 is not observed. This is confirmed by X-ray diffraction analysis of this specimen, in which no SiO_2 peak was detected as shown in Fig. 7.

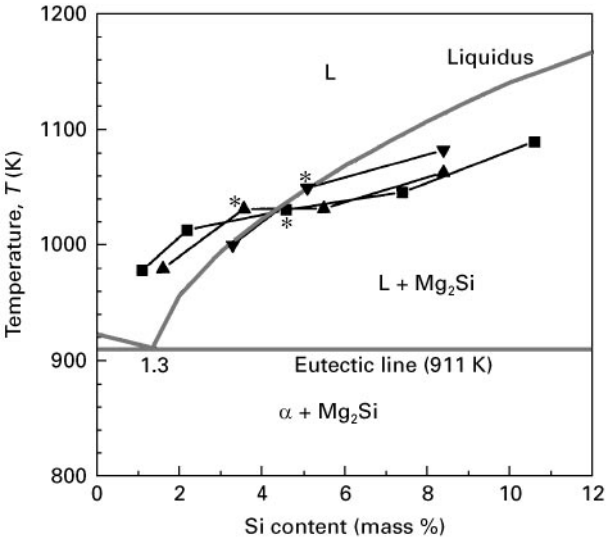

Figure 14 Measured infiltration-front temperatures plot against the average Si contents in each system on the Mg–Si phase diagram. For SiC_p diameters of: (■) 8 μm, (▲) 3 μm and (▼) 2 μm. *L* = liquid.

In order to clarify the macroscopic behaviour of Mg_2Si crystallization with various SiO_2 contents, the Mg–Si phase diagram is considered. By assuming that the Mg–SiO_2 reaction finishes in a moment at the infiltration front and that microsegregation of Si at the front is ignored (i.e. the Si content in the matrix metal is always the average composition of the system), measured infiltration-front temperatures can be plotted on the Mg–Si phase diagram against the average Si contents, which are calculated from the data in Table II. The results are shown in Fig. 14, where three

points of 15 mass % SiO_2 are marked with asterisks (*). From this figure, 15 mass % SiO_2 is the threshold value, and above this SiO_2 content, the infiltration-front temperature becomes lower than the liquids. This means that the amount of Mg_2Si that crystallizes during infiltration abruptly increases above 15 mass % SiO_2, resulting in strong disturbance of the infiltration. Therefore, it is concluded that the major factor influencing the steep drop in infiltration velocity is the disturbance caused by the crystallization of Mg_2Si during infiltration.

The effect of SiO_2 content on infiltration velocity, therefore, is defined by the increasing infiltration-front temperature caused by the increasing SiO_2 content (an accelerating factor), and by the formation of increasing amounts of MgO and Mg_2Si disturbing the infiltration (the decelerating factors).

5. Conclusions

To apply a spontaneous infiltration phenomenon to the fabrication of magnesium matrix composites, a new method was developed. In this study, fundamental experiments to clarify the conditions necessary for spontaneous infiltration were carried out, and the infiltration behaviour was discussed. The following conclusions were obtained.

1. By mixing SiO_2 powder (infiltration agent) with SiC_p powder (reinforcement), spontaneous infiltration of the magnesium melt into the powder mixture becomes possible under a pure argon atmosphere at 973 K.

2. A minimum SiO_2 content necessary for spontaneous infiltration exists, and it depends on the SiC_p diameter.

3. For spontaneous infiltration, holes on the bottom of the crucible are needed.

4. SiC particle distribution in the composite is homogeneous without any agitation, even given the fine SiC particle size.

5. Spontaneous infiltration is caused by the improvement of wettability between the magnesium melt and the SiC particle, which results from high temperature Mg–SiO_2 thermit reaction at the infiltration front.

6. The Infiltration velocities have maxima at 15 mass % SiO_2 for 3, 4 and 8 μm SiC_p powders.

7. The factors accelerating the infiltration velocity are the increasing infiltration-front temperature due to increasing SiO_2 content and the increasing hydraulic radius due to increasing SiC_p diameter.

8. The factors that decelerate the infiltration velocity are the two reaction products, MgO and Mg_2Si. The formation of increasing amounts of MgO with increasing SiO_2 content, gradually disturbs the infiltration. However, Mg_2Si has a discontinuous disturbing effect with SiO_2 content.

9. The effect of the SiO_2 content on the infiltration velocity is defined by a combination of these factors.

References

1. M. O. PEKGULERYUZ, in "Magnesium composites – a critical review' (Institute of Magnesium Technology, Québec).
2. A. LUO and M. O. PEKGULERYUZ, in Proceedings of 51st International Magnesium Association Congress, Berlin, May 1994 (International Magnesium Association, USA, 1994) p. 74.
3. P. ROHATGI, *J. Met.* **43** (1991) 10.
4. V. LAURENT, P. JARRY, G. REGAZZONI and D. APELIAN, *J. Mater. Sci.* **27** (1992) 4447.
5. M. D. SKIBO and D. M. SCHUSTER, US Patent 4 759 995, July (1988).
6. K. U. KAINER, *Proceedings of the International Conference of ASME* **37** (1991) 191.
7. M. K. AGHAJANIAN and J. T. BURKE, in Proceedings of the 34th International SAMPE Symposium, May 1989 (1989) p. 817.
8. M. K. AGHAJANIAN, M. A. ROCAZELLA, J. T. BURKE and S. D. KECK, *J. Mater. Sci.* **26** (1991) 447.
9. J. T. BURKE, M. K. AGHAJANIAN and M. A. ROCAZELLA, in Proceedings of the 34th International SAMPE Symposium, May 1989 (1989) p. 2440.
10. Y. CHEN and D. D. L. CHUNG, in Proceedings on Processing and Fabrication of Advanced Materials III, edited by V. A. Ravi, T. S. Srivatsan and J. J. Moore, (The Minerals, Metals and Materials Society, USA, 1994) p. 795.
11. I. BARIN, in "Thermochemical data of pure substances" (VCH, 1993) p. 883.
12. G. P. MARTINS, D. L. OLSON and G. R. EDWARDS, *Metall. Trans.* **19B** (1988) 95.
13. P. B. MAXWELL, G. P. MARTINS, D. L. OLSON and G. R. EDWARDS, *ibid.* **21B** (1990) 475.
14. SUK-WON LIM and TAKAO CHOH, *J. Jpn. Inst. Metals* **56** (1992) 210.
15. K. A. SEMLAK and F. N. RHINES, *Trans. AIME* **212** (1958) 325.
16. S-Y. OH, J. A. CORNIE and K. C. RUSSELL, *Proc. Ceram. Engng Sci.* **8** (1987) 912.

Received 15 August 1995
and accepted 17 July 1996